ELSEVIER

Journal of Alloys and Compounds 298 (2000) 51–58

Journal of ALLOYS AND COMPOUNDS

www.elsevier.com/locate/jallcom

Magnetism and transport properties of HfMSi (M=Pt, Pd) and $HfRh_{1-x}Pd_xSi$

S. Yashiro[a], Y. Nagata[a], H. Samata[b], S. Abe[c]

[a]*College of Science and Engineering, Aoyama Gakuin University, Chitosedai, Setagaya, Tokyo 157-8572, Japan*
[b]*Faculty of Mercantile Marine Science, Kobe University of Mercantile Marine, 5-1-1 Fukaeminami, Higashinada, Kobe 658-0022, Japan*
[c]*Department of Electrical Engineering, Kanagawa University, 3-27 Rokkakubashi, Kanagawa-ku, Yokohama, Kanagawa 221, Japan*

Received 8 October 1999; accepted 14 October 1999

Abstract

The crystallographic, electric, and magnetic properties of the new intermetallic compounds HfMSi (M=Pt or Pd) and the superconductivity of $HfRh_{1-x}Pd_xSi$ were studied. The crystal structure of HfPtSi and HfPdSi could be refined assuming an orthorhombic structure (space group *Pnma*) and lattice constants of $a=0.6549$ nm, $b=0.3883$ nm, and $c=0.7506$ nm for HfPtSi and $a=0.6570$ nm, $b=0.3874$ nm, and $c=0.7565$ nm for HfPdSi. Both compounds are metallic and show diamagnetic behavior below 300 K. A small effective electron mass is thought to be a reason for the diamagnetism of HfMSi (M=Pt or Pd). In the $HfRh_{1-x}Pd_xSi$ system, the superconductivity of HfRhSi ($T_c=2.2$ K) is suppressed by replacing Rh by Pd. The Pd content dependence of the Pauli paramagnetic susceptibility suggests that reduction of the density of states at the Fermi level is a possible cause of the suppression of superconductivity in the $HfRh_{1-x}Pd_xSi$ system.

Keywords: Intermetallic compounds; Crystallographic property; Electric resistivity; Superconductivity

1. Introduction

The discovery of superconductivity in Y–Ni–B–C and Y–Pd–B–C systems [1–3] stimulated the search for new high-T_c intermetallic compounds. Many studies have been done to discover new intermetallic compound superconductors in borocarbide systems that contain rare earth and transition metal elements. If a new high-T_c superconductor is discovered in an intermetallic system, superconductivity will be used more widely since the processing technology of the intermetallic compounds has been established. The transition temperature of intermetallic compounds, however, still remains at lower temperatures (<23 K). The development of new intermetallic compounds seems crucially important for using metallic superconductors at high temperatures above 20 K. Therefore, a continuous search for new intermetallic superconductors must be conducted by using various constituent elements.

Among the variety of intermetallic systems, transition metal silicides and germanides are interesting because some of their compounds display various interesting properties such as mixed valence, antiferromagnetic and ferromagnetic ordering, and Kondo lattice formation [4,5]. We have investigated the ternary intermetallic compound systems of Hf–M–Ge (M=3d, 4d or 5d transition metals) and discovered some new intermetallic compounds such as $Hf_3Ni_4Ge_4$ and HfPtGe [6]. Although these compounds were not superconductors, superconductivity with a transition temperature of 2.3 K has been reported for HfRhSi by Shirotani et al. [7]. Transition metal germanides and silicides seem to be interesting systems in the search for new superconducting intermetallic compounds. In this study, we investigated the Hf–M–Si (M=Pt, Pd) system and discovered new compounds of HfPtSi and HfPdSi. In this paper, their crystallographic, electric, and magnetic properties, and as well as the superconductivity of the solid solution between HfRhSi and HfPdSi are reported.

2. Experimental method

Polycrystalline specimens of HfMSi (M=Pt, Pd) were prepared by arc-melting and subsequent heat treatment. A stoichiometric composition of Hf (99.9%), Si (99.9999%), and Pt (99.99%) or Pd (99.9%) was melted in an arc-

E-mail address: ynaga@ee.aoyama.ac.jp (Y. Nagata)

0925-8388/00/$ – see front matter
PII: S0925-8388(99)00649-0

furnace using a zirconium-gettered argon atmosphere. The mixture was sealed into a quartz ampoule with argon gas (230 Torr) after being evacuated to 5×10^{-5} Torr. The encapsulated mixture was heated to 700°C in an electric furnace. An inner argon gas pressure of 760 Torr was established at 700°C. After being maintained at that temperature for 3 days, the ampoule was quenched in water. Specimens of $HfRh_{1-x}Pd_xSi$ ($0\leqq x\leqq 1$) were prepared by the same procedure as that used for preparing specimens of HfMSi using Rh (99.99%) in addition to high-purity Hf, Pd, and Si.

The chemical composition of the compound was determined by electron-probe micro-analysis (EPMA) using wave-length dispersive spectrometers. A crystallographic analysis was performed by X-ray powder diffraction using Cu Kα radiation and subsequent refinement of the diffraction data using the Rietveld method. Electrical resistivity was measured by a conventional DC four-probe method at temperatures from 10 to 300 K. Electrical leads were made by spot-welding gold wires (50 μm) onto a polished surface of the specimen. Magnetic measurements were performed using a SQUID magnetometer at temperatures between 1.7 and 300 K in an applied magnetic field up to 10 kOe.

3. Results and discussion

3.1. Properties of HfMSi (M=Pt, Pd)

3.1.1. Crystallographic properties of HfMSi (M=Pt, Pd)

Single phase specimens were obtained when an as-melt specimen was annealed at 700°C for 3 days. The chemical composition of the specimens was determined to be HfPtSi and HfPdSi by micro-analysis using EPMA. Fig. 1a,b, respectively, show the results of X-ray powder diffraction and the refinement of the diffraction data for of HfPtSi and HfPdSi. When an orthorhombic structure in space group *Pnma* and lattice constants of $a=0.6549$ nm, $b=0.3883$ nm, and $c=0.7506$ nm for HfPtSi and $a=0.6570$ nm, $b=0.3874$ nm, and $c=0.7565$ nm for HfPtSi were assumed, the diffraction data could be refined. The crystallographic parameters obtained by the refinement are listed in Tables 1 and 2for HfPtSi and HfPtSi, respectively. The structure of these compounds is the same as those of HfPtGe and superconducting HfRhSi [6,7].

3.1.2. Electric resistivity of HfMSi (M=Pt, Pd)

Fig. 2 shows the temperature dependence of the electrical resistivity of HfPtSi and HfPdSi. The $\rho(T)$ shows the metallic behavior, and the resistivity decreases as the temperature decreases. Superconductivity was not observed down to 1.5 K. Although both specimens are single-phase according to the results of X-ray diffraction, their residual resistivity is considerably large, suggesting the existence of some impurities in the specimens. The

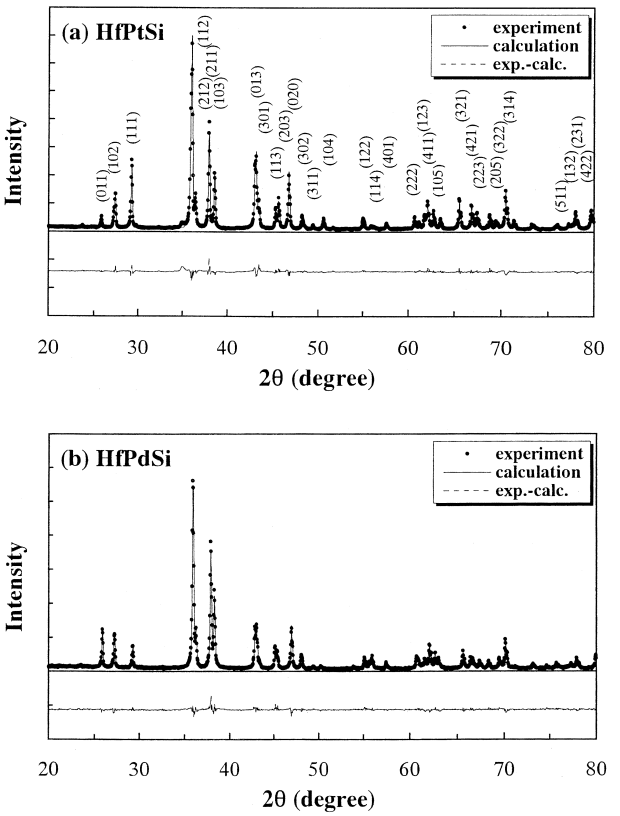

Fig. 1. The results of X-ray powder diffraction and the refinement of the diffraction data for the specimens of (a) HfPtSi and (b) HfPdSi.

Table 1
Crystal structure parameters of HfPtSi[a]

Atom	Atomic parameters			
	Site	*x*	*y*	*z*
Hf	4*c*	0.0257	1/4	0.1779
Pt	4*c*	0.1448	1/4	0.5631
Si	4*c*	0.7573	1/4	0.6223

[a] Space group, *Pnma*, orthorhombic; lattice parameters, $a=0.6549$ nm, $b=0.3883$ nm, $c=0.7506$ nm; structure type, Co_2Si; and density, 13.98 g/cm^3.

resistivity $\rho(T)$ can be described by a modified parallel resistor model. According to the parallel resistor model [8,9], $\rho(T)$ is given by

Table 2
Crystal structure parameters of HfPdSi[a]

Atom	Atomic parameters			
	Site	*x*	*y*	*z*
Hf	4*c*	0.0274	1/4	0.1815
Pd	4*c*	0.1426	1/4	0.5590
Si	4*c*	0.7645	1/4	0.6312

[a] Space group, *Pnma*, orthorhombic; lattice parameters, $a=0.6570$ nm, $b=0.3874$ nm, $c=0.7565$ nm; structure type, Co_2Si; and density, 10.80 g/cm^3.

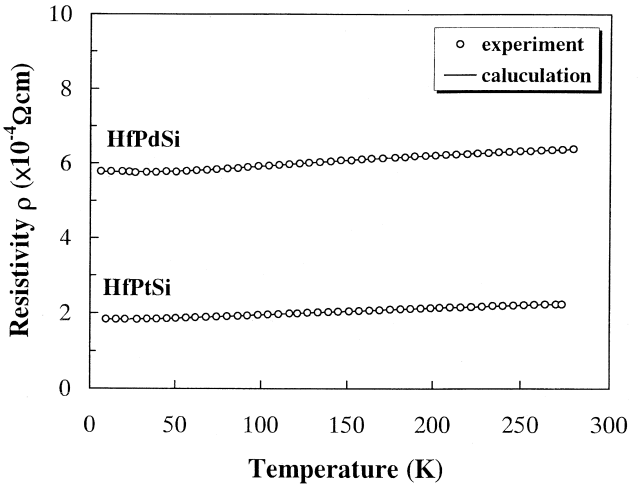

Fig. 2. Temperature dependence of the electrical resistivity for the specimens of HfPtSi and HfPdSi. The solid lines show the results of calculation.

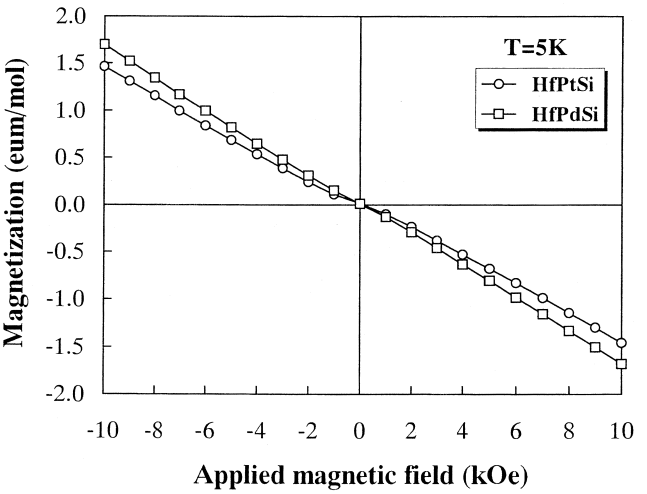

Fig. 3. Magnetic field dependence of the magnetization for the specimens of HfPtSi and HfPdSi measured at 5 K.

$$\frac{1}{\rho(T)} = \frac{1}{\rho_{rp}(T)} + \frac{1}{\rho_{max}}, \quad (1)$$

where $\rho_{rp}(T)$ is the sum of the residual resistivity ρ_0 and phonon-assisted resistivity $\rho_{ph}(T)$ and ρ_{max} is the saturation resistivity, which is independent of the temperature. Although Wiesmann et al. [8] have used $\rho_{ph}(T)$ which is based on the Debye model, the model has been modified according to the Bose–Einstein statistics in this study. When it is assumed simply that the phonon scattering of conduction electrons is due to a thermal phonon with a flat energy distribution between E_1 and E_2, $\rho_{ph}(T)$ can be derived by assuming that $\rho_{ph}(T)$ satisfies the Bose–Einstein statistics as

$$r_{ph}(T) = \alpha[(E_1 - E_2)/k_B + T \ln\{(e^{E_2/k_BT} - 1)/(e^{E_1/k_BT} - 1)\}] \quad (2)$$

where α and k_B are the fitting coefficient and the Boltzmann constant [10]. Experimental $\rho(T)$ data were fitted by Eq. (2), and results of the fitting are shown in Fig. 2 by solid lines. Phonon excitation energies of $E_1 = 11.4$ meV and $E_2 = 12.6$ meV and $E_1 = 15.0$ meV and $E_2 = 22.7$ meV were obtained by the fitting for HfPtSi and HfPdSi, respectively. Since the difference between E_1 and E_2 is very small, thermal phonons with an energy of 12 meV (~140 K) to 19 meV (~220 K) may contribute to $\rho_{ph}(T)$ of HfPtSi and HfPdSi, respectively. In the study of LaPtSi, a Debye temperature Θ_D of 250 K (~22 meV) has been reported [11]. Although the crystal structure of HfMSi (M = Pt, Pd) is slightly different from that of LaPtSi, the phonon excitation energy of HfMSi seems reasonable in comparison with the Θ_D of LaPtSi.

3.1.3. Magnetic properties of HfMSi (M = Pt, Pd)

Fig. 3 shows the magnetic field dependence of the magnetization measured at 5 K for specimens of HfPtSi and HfPdSi. The $M(H)$ data show an almost linear field dependence with negative slope, indicating diamagnetism of the compounds. Fig. 4a,b show the temperature dependence of the molar magnetic susceptibility of HfPtSi and HfPdSi, respectively. Susceptibility was measured by applying a magnetic field of 10 kOe. The magnetic susceptibility $\chi(T)$ of both compounds shows diamagnetic behavior over the whole temperature range measured. However, the susceptibility of both compounds increases considerably when the temperature decreases below 50 K. The $\chi(T)$ of HfPtSi can be explained by the relation $\chi(T) = \chi_0 + C_{mol}/(T - \Theta)$, where χ_0, Θ and C_{mol} are the temperature-independent magnetic susceptibility, the paramagnetic Curie temperature, and the Curie constant, respectively. The temperature-independent susceptibility χ_0 was determined to be -1.33×10^{-4} emu/mol by fitting the above equation to the data. The χ_0 seems to be an intrinsic magnetic susceptibility of HfPtSi. Although it is difficult to give an exact explanation of the diamagnetism of HfPtSi, a possible reason of the diamagnetism can be derived from qualitative arguments. In general, the magnetic susceptibility of metal is given by $\chi_0 = \chi_c + \chi_P + \chi_L$ and χ_L is given by $\chi_L = -(m/m^*)^2 \chi_P/3$, where χ_c, χ_P, χ_L, m and m^* are the core diamagnetism, Pauli paramagnetism, Landau diamagnetism, electron mass, and effective electron mass, respectively [12]. Consequently, χ_0 is represented by

$$\chi_0 = \chi_c + \left[1 - \frac{1}{3}\left(\frac{m}{m^*}\right)^2\right]\chi_P \quad (3)$$

where the Stoner enhancement factor has been assumed to be 1. The core diamagnetic susceptibility χ_c is determined to be -5.7×10^{-5} emu/mol by assuming the valences of Hf, Pt, and Si as 4, 2 and 4, respectively. By subtracting χ_c from χ_0, the resultant $\chi_0 - \chi_c$ is determined to be -7.6×10^{-5} emu/mol. Since the Pauli paramagnetic susceptibility χ_P has a positive value, the relation $m^* < m\sqrt{3}$ must be

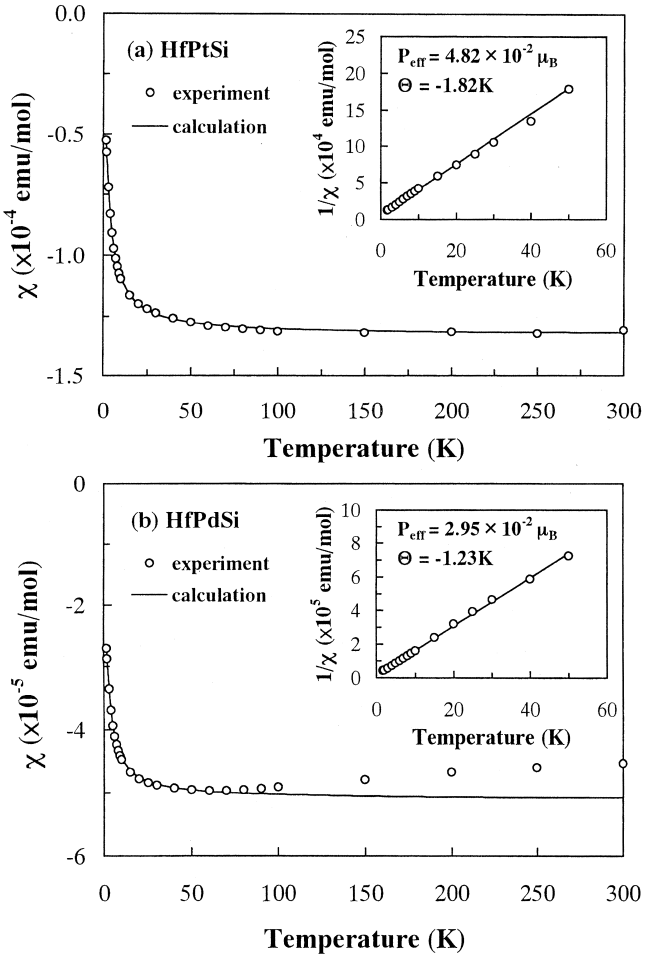

Fig. 4. Temperature dependence of the molar magnetic susceptibility measured for the specimens of (a) HfPtSi and (b) HfPdSi at 10 kOe. The insets of the figures show temperature dependence of the reciprocal susceptibility $\chi_r(T)^{-1}=(\chi(T)-\chi_0)^{-1}$.

satisfied to explain the negative value of $\chi_0-\chi_c$. Therefore, a small effective electron mass seems to be a possible reason for the diamagnetism of HfPtSi. It is known that a small effective mass occurs when the Fermi surface lies in a region at the boundary of a Brillouin zone [13]. The shape and relative configuration of the Brillouin zone and the Fermi surface may be a reason for the small effective mass of HfPtSi.

When χ_0 is subtracted from $\chi(T)$, the residual susceptibility $\chi_r(T)=\chi(T)-\chi_0$ shows paramagnetic behavior. The temperature dependence of the reciprocal susceptibility χ_r^{-1} is shown in the inset of Fig. 4a. The reciprocal susceptibility $\chi_r^{-1}(T)$ shows a linear temperature dependence, and the data can be fitted by the Curie–Weiss law that is given by $1/\chi_{mol}=(T-\Theta)/C_{mol}$. $\Theta=-1.82$ K and $C_{mol}=2.88\times10^{-4}$ emu/mol were obtained by the fitting. The result of the fitting is shown by the solid line in the inset of Fig. 4a. The effective magnetic moment P_{eff}, which is thought to be due to the paramagnetic impurity, is deduced as 4.8×10^{-2} μ_B/formula unit from the Curie constant C_{mol}. Although a negative value was obtained for Θ, the temperature-dependent susceptibility χ_r could be attributed to a paramagnetic impurity in the specimen.

The $\chi(T)$ curve of HfPdSi (Fig. 4b) resembles that of HfPtSi at low temperatures. However, $\chi(T)$ shows a peculiar behavior at temperatures above 50 K and tends to increase monotonically as the temperature increases. The $\chi(T)$ data at temperatures below 50 K was fitted by the same relation $\chi(T)=\chi_0+C_{mol}/(T-\Theta)$ as that used for HfPtSi and $\chi_0=-5.1\times10^{-5}$ emu/mol was obtained. The core susceptibility χ_c of HfPdSi is estimated as -4.2×10^{-5} emu/mol assuming the valences of Hf, Pd, and Si as 4, 2, and 4, respectively. Subsequently, $\chi_0-\chi_c$ is determined to be -0.9×10^{-5} emu/mol. The $\chi_0-\chi_c$ is attributed to the contribution of χ_P and χ_L. In order to explain this negative residual susceptibility, $\chi_L<\chi_P$ and then $m^*<m$ must be satisfied as in the case of HfPtSi. Therefore, the diamagnetism of HfPdSi is also considered to be due to the small effective electron mass. On the other hand, the residual susceptibility $\chi_r(T)=\chi(T)-\chi_0$ shows paramagnetic behavior below 50 K. The temperature dependence of the reciprocal of χ_r is shown in the inset of Fig. 4b. The $\chi_r^{-1}(T)$ shows a linear temperature dependence at temperatures below 50 K, and the data can be fitted by the Curie–Weiss law. The result of the fitting is shown by the solid line in the inset of Fig. 4b. $\Theta=-1.23$ K and $C_{mol}=7.17\times10^{-5}$ emu/mol were obtained by the fitting. The effective paramagnetic moment P_{eff} deduced from C_{mol} is 2.95×10^{-2} μ_B/f.u. Although a small negative value was obtained for Θ, as in the case of HfPtSi, χ_r can be attributed to a paramagnetic impurity in the specimen.

3.2. Superconductivity of $HfRh_{1-x}Pd_xSi$

3.2.1. Crystallographic properties

Specimens with the chemical compositions of $HfRh_{1-x}Pd_xSi$ ($0\leqq x\leqq1$) were prepared, and their superconductivity and magnetism were studied. X-ray powder diffraction data could be refined when an orthorhombic structure in a space group *Pnma* was assumed. Fig. 5 shows the Pd content dependence of the orthorhombic lattice constants of $HfRh_{1-x}Pd_xSi$. Since HfPdSi has the same crystal structure as that of HfRhSi, the system $HfRh_{1-x}Pd_xSi$ appears to form a solid solution, and the lattice constants show a monotonous change with increasing Pd content. The lattice constants *a* and *c* increase, while the constant *b* decreases. Since the increase in *c* is larger than those of *a* and *b*, Pd substitution is thought to increase lattice spacing along the *c*-axis, and then increases the cell volume from 0.1868 to 0.1925 nm^3 as the Pd content increases.

3.2.2. Superconducting properties of $HfRh_{1-x}Pd_xSi$

It has been reported that HfRhSi shows superconductivity at 2.3 K [7]. However, the superconducting parameters

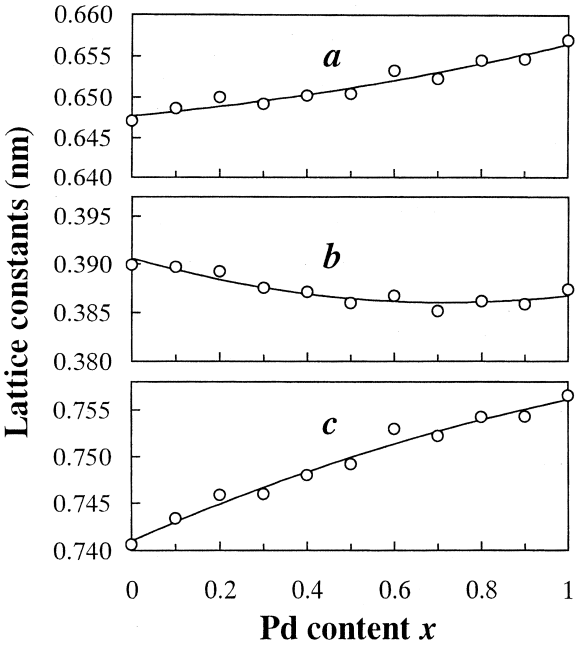

Fig. 5. Pd content dependence of orthorhombic lattice constants of $HfRh_{1-x}Pd_xSi$.

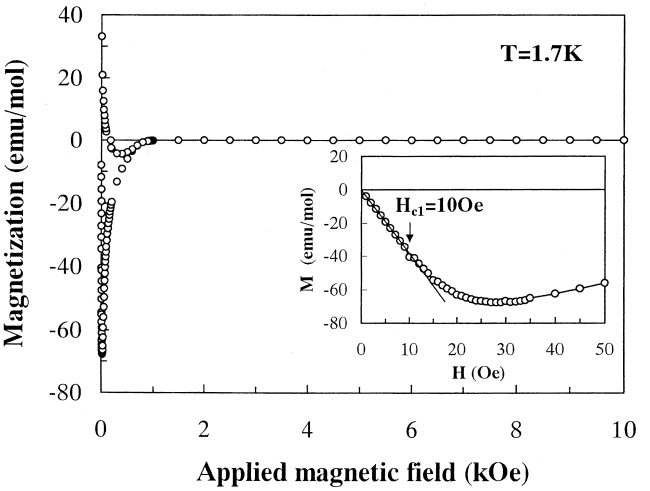

Fig. 7. Magnetic field dependence of the magnetization for a specimen of HfRhSi at 1.7 K. The inset of the figure shows the magnetic field dependence of the magnetization at lower magnetic fields.

of HfRhSi are as yet unclear. Prior to the investigation of the substitution effect in the $HfRh_{1-x}Pd_xSi$ system, the superconductivity of HfRhSi was characterized by means of magnetization measurements. Fig. 6 shows the temperature dependence of magnetization measured for a specimen of HfRhSi in various magnetic fields. The onset of the superconducting transition was observed at 2.2 K under a magnetic field of 1 Oe, and the onset shifts to low temperatures as the magnetic field increases. The upper critical field H_{c2} at a given temperature was estimated by using the $M(T)$ data shown in Fig. 6. The transition temperature in a given field was defined as onset of the superconducting transition. Fig. 7 shows the magnetic field dependence of the magnetization for a specimen of HfRhSi at 1.7 K. A paramagnetic contribution has been subtracted from the raw data. The magnetization shows the typical behavior of superconductors and looks almost constant at fields above 2 kOe. As shown in the inset of Fig. 7, the lower critical field H_{c1} at 1.7 K was determined to be 10 Oe. The H_{c1} were also determined at 1.8, 1.9, 2.0 and 2.1 K. H_{c1} and H_{c2} are shown in Fig. 8a,b, respectively, as a function of temperature. Both critical fields increase rapidly as the temperature decreases. Although the data are not sufficient because of the low T_c of HfRhSi, $H_{c1}(0)$ and $H_{c2}(0)$ can be estimated by extrapolating the data to $T=0$

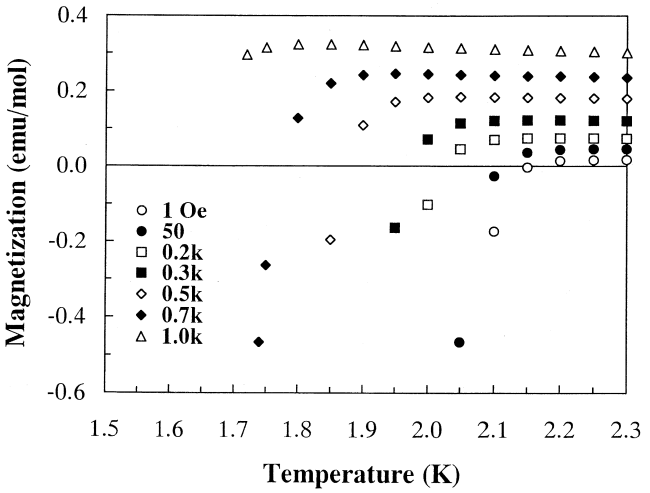

Fig. 6. Temperature dependence of the magnetization measured for a specimen of HfRhSi in various magnetic fields.

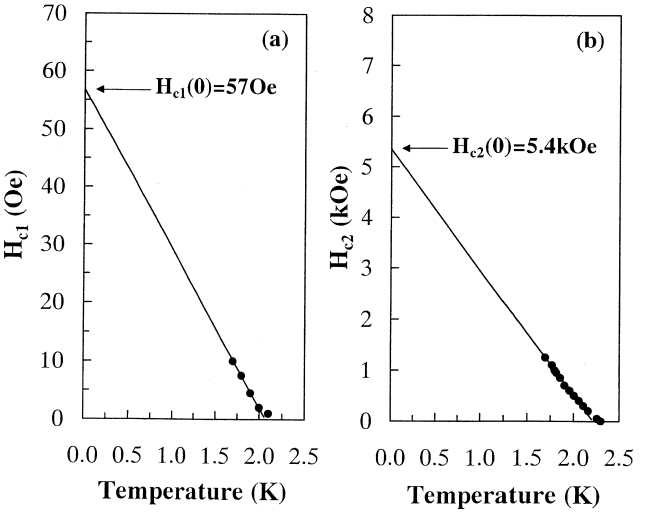

Fig. 8. Temperature dependence of H_{c1} and H_{c2} for a specimen of HfRhSi.

K. $H_{c1}(0)=57$ Oe and $H_{c2}(0)=5.4$ kOe were obtained by linear extrapolation. The Ginzburg–Landau (G-L) coherence length $\xi_{GL}(0)$ was determined as 25 nm using the value of $H_{c2}(0)$ and the relation $H_{c2}(0)=\Phi_0/2\pi\xi^2_{GL}$, where Φ_0 is the flux quantum. The G-L penetration depth of $\lambda_{GL}=340$ nm was deduced from the relation $\lambda_{GL}=[\Phi_0/\pi H_{c1}(0)]^{1/2}$ using the values of $H_{c1}(0)$. The G-L parameter κ is a good measure to characterize the type of superconductivity, and the κ is given by $\kappa=\lambda_{GL}/\xi_{GL}$. Using the values of λ_{GL} and ξ_{GL}, $\kappa=14$ was obtained. Since the G-L parameter κ is larger than $1/\sqrt{2}$, HfRhSi is thought to be a type II superconductor. The electronic-specific heat coefficient γ can be estimated by using the value of $\xi_{GL}(0)$ and the relation $\gamma=7.34\times10^{-13}/\xi_{GL}(0)^2\rho T_c$, where ρ is the resistivity just above T_c. γ was determined as 1220 erg/cm^3 K^2 (3.42 mJ/mol·K^2) using the value of ρ which is shown later in Fig. 11. The enhanced density of states $N(E_F)_{en}$ at the Fermi level can be also estimated using the relation $N(E_F)_{en}=0.2121\gamma/N$, where N is the number of atoms per formula unit and γ is expressed in mJ/mol·K^2. $N(E_F)_{en}=0.242$ states/eV·atom·spin was deduced. In spite of different crystal structure, the superconducting parameters obtained for HfRhSi in this study are very similar to those of LaPtSi [11].

Fig. 9 shows the temperature dependence of molar magnetic susceptibility for the specimens with $x=0$, 0.1, 0.2 and 0.3 measured in an applied magnetic field of 5 Oe. When Rh is replaced by Pd, the onset temperature of the superconducting transition shifts to lower temperature. The inset of Fig. 9 shows the Pd content dependence of superconducting transition temperature T_c, which was determined as the onset of the superconducting transition. The transition temperature T_c decreases monotonically as the Pd content x increases, and the superconducting transition cannot be observed at temperatures down to 1.5 K for specimens with a Pd content longer than $x=0.3$. The Pd substitution seems to suppress the superconductivity of HfRhSi. Since the T_c of HfRhSi is too low, the substitution effect to the superconducting parameters, except T_c, could not be characterized in this study.

3.2.3. Magnetic properties

The temperature dependence of the molar magnetic susceptibility that was measured in a magnetic field of 10 kOe is shown in Fig. 10. The $\chi(T)$ curves have hardly any temperature dependence at temperatures above 20 K. However, a small temperature dependence is observed at higher temperatures below 20 K. This behavior is attributed to the presence of paramagnetic impurities in the specimen. The $\chi(T)$ curves can be explained by the relation $\chi(T)=\chi_0+C_{mol}/(T-\theta)$. The temperature-independent χ_0 obtained by fitting the equation to the experimental $\chi(T)$ is shown in Fig. 11 as a function of Pd content x. Although the χ_0 has a positive value for the specimens with $x\leqq0.6$, it decreases and changes its sign to negative as the Pd content increases. The temperature-independent susceptibility χ_0 is represented by Eq. (3), and the core diamagnetic susceptibility χ_c of $HfRh_{1-x}Pd_xSi$ is given by the relation $\chi_c(x)=\chi_{Hf}+(1-x)\chi_{Rh}+x\chi_{Pd}+\chi_{Si}$, where χ_{Hf}, χ_{Rh}, χ_{Pd}, and χ_{Si} are the diamagnetic susceptibility of Hf, Rh, Pd, and Si, respectively. As shown in Fig. 11, the residual susceptibility $\chi_0-\chi_c$, obtained by assuming the valences of Hf, Rh, Pd, and Si as 4, 3, 2 and 4, respectively, has a positive value for specimens with the compositions $x\leqq0.7$. However, $\chi_0-\chi_c$ decreases with increasing Pd content x, and when the Pd content x increases above $x=0.7$, $\chi_0-\chi_c$ changes its sign from positive to negative. According to Eq. (3), the relation $0<m/m^*<\sqrt{3}$ must be satisfied to explain the positive

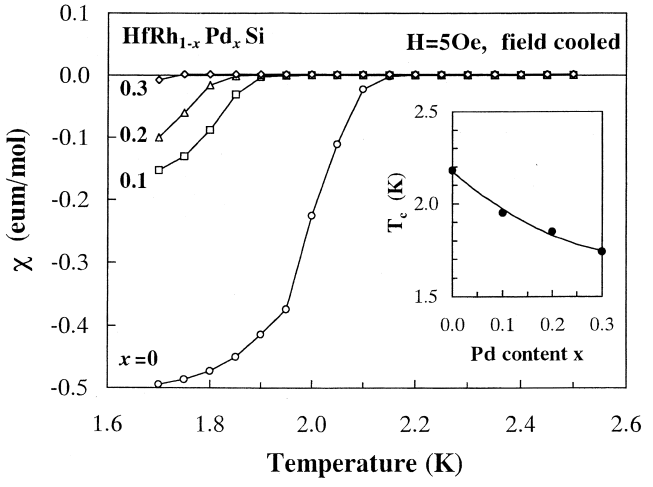

Fig. 9. Temperature dependence of molar magnetic susceptibility measured for the specimens of $HfRh_{1-x}Pd_xSi$ in an applied magnetic field of 5 Oe. The inset of the figure shows the Pd content dependence of the superconducting transition temperature T_c.

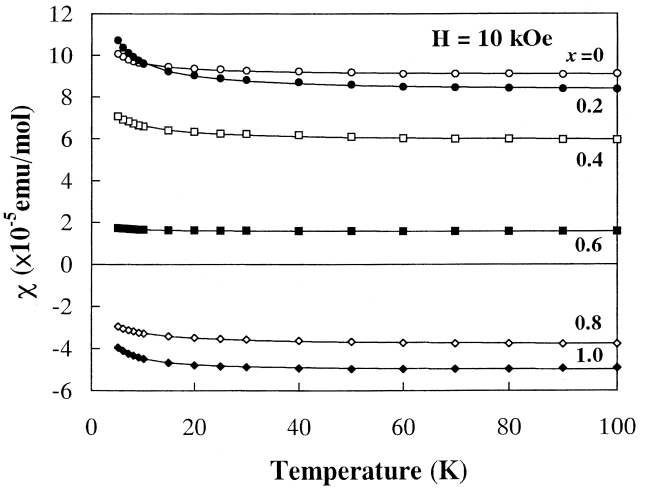

Fig. 10. Temperature dependence of molar magnetic susceptibility measured for the specimens of $HfRh_{1-x}Pd_xSi$ in an applied magnetic field of 10 kOe.

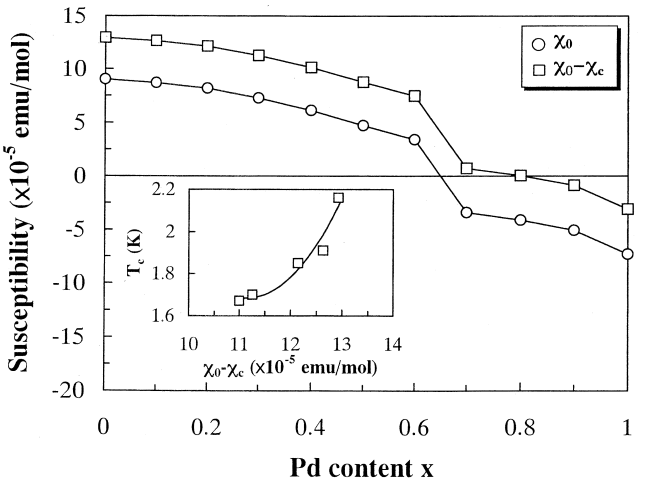

Fig. 11. Pd content dependence of the temperature-independent susceptibility χ_0 and $\chi_0-\chi_c$, where χ_c is the core susceptibility. The inset of the figure shows superconducting transition temperature T_c as a function of $\chi_0-\chi_c$.

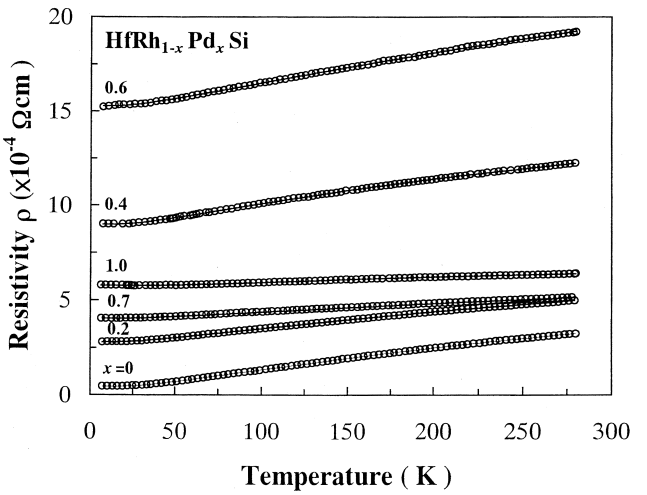

Fig. 12. Temperature dependence of the electrical resistivity for the specimens of $HfRh_{1-x}Pd_xSi$.

$\chi_0-\chi_c$ values observed for specimens with $x \leqq 0.7$. In this case, there is high potential that a situation with $m^*>m$ occurs. On the contrary, the relation $m/m^*>\sqrt{3}$ must be satisfied to explain the negative $\chi_0-\chi_c$ observed for specimens with $x>0.7$, and in this case $m^*<m$ must be established. The change in the effective electron mass may be a reason why $\chi_0-\chi_c$ changes its sign from positive to negative at about $x=0.7$. A change in the shape and the relative configuration of the Brillouin zone and the Fermi surface may occur along with the Pd substitution. Since $\chi_0-\chi_c$ is considered to be equivalent to the Pauli paramagnetic susceptibility χ_P and χ_P is proportional to $D(E_F)$, which is the density of state at the Fermi level, the Pd content dependence of $\chi_0-\chi_c$ would be analogous to that of $D(E_F)$. Therefore, $D(E_F)$ is considered to decrease with increasing Pd content. The inset of Fig. 11 shows the superconducting transition temperature T_c of $HfRh_{1-x}Pd_xSi$ as a function of $\chi_0-\chi_c$. The decrease in $\chi_0-\chi_c$, which means a decrease in $D(E_F)$, seems to suppress the superconductivity of HfRhSi and to decrease the transition temperature T_c. Presumably, HfRhSi belongs to the category of BCS superconductors. Since the superconductivity of the BCS superconductors depends on the state density at the Fermi level, the reduction of $D(E_F)$ is a possible reason for the suppression of superconductivity observed for $HfRh_{1-x}Pd_xSi$ ($x<0.4$). The reduction of $D(E_F)$ may be correlated with the expansion of cell volume. However, further details are not available at present. When $\chi_0(x)$ is subtracted from $\chi(T)$ of the specimens with various Pd content x, the residual susceptibility $\chi(T)-\chi_0(x)$ shows typical paramagnetic characteristics. This behavior could be due to a paramagnetic impurity in the specimen, similarly to the behavior of $\chi(T)-\chi_0$ observed for specimens of HfMSi (M=Pt, Pd).

3.2.4. Normal-state electrical resistivity

Fig. 12 shows the temperature dependence of the electrical resistivity measured for specimens of $HfRh_{1-x}Pd_xSi$. All specimens show typical metallic behavior above 5 K. The $\rho(T)$ data for the specimens with various Pd content can be explained by Eq. (1), which was used to explain $\rho(T)$ of HfMSi (M=Pt, Pd). The results of the fitting are shown in Fig. 12 by solid lines. The mean value $(E_1+E_2)/2$ of the phonon excitation energies and the residual resistivity ρ_0, which were obtained by the fitting, is shown in Fig. 13. It is seen that the excitation energy has an energy of 7.5–10 meV for specimens with $x<0.9$. Presumably, thermal phonons with an energy of about 8 meV contribute to the resistivity $\rho_{ph}(T)$ of $HfRh_{1-x}Pd_xSi$ system. On the other hand, ρ_0 increases as the Pd content increases and shows a remarkable change at the com-

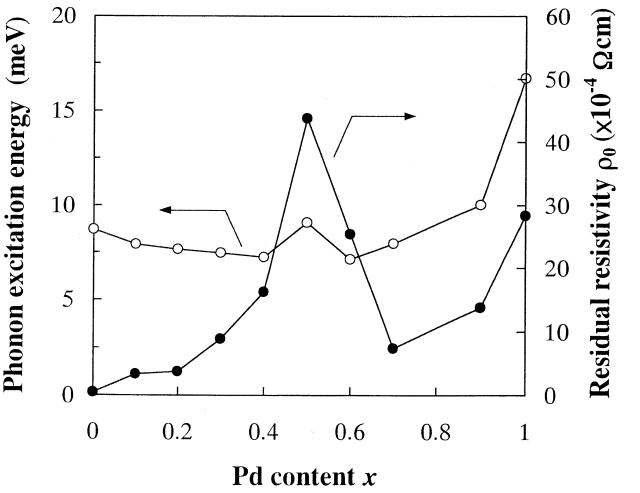

Fig. 13. Phonon excitation energy $(E_1+E_2)/2$ and residual resistivity ρ_0 as a function of Pd content x.

position $x=0.6$. This composition corresponds to the composition at which χ_0 changes its sign from positive to negative. However, the reason for this behavior is presently unclear.

4. Conclusion

The crystallographic, electric, and magnetic properties of the new intermetallic compounds HfMSi (M=Pt or Pd) and the superconductivity of $HfRh_{1-x}Pd_xSi$ were studied. The crystal structure of HfPtSi and HfPdSi could be refined assuming an orthorhombic structure (space group *Pnma*) and the lattice constants of $a=0.6549$ nm, $b=0.3883$ nm, and $c=0.7506$ nm for HfPtSi and $a=0.6570$ nm, $b=0.3874$ nm, and $c=0.7565$ nm for HfPdSi. Both compounds show metallic transport properties and diamagnetic behavior below 300 K. A small effective electron mass is thought to be the reason for the diamagnetism of HfMSi (M=Pt or Pd). In the $HfRh_{1-x}Pd_xSi$ system, the superconductivity of HfRhSi ($T_c=2.2$ K) is suppressed by the substitution of Pd for Rh. The Pd content dependence of the temperature-independent magnetic susceptibility suggests that the reduction of the density of states at the Fermi level is a possible cause of the suppression of superconductivity in the $HfRh_{1-x}Pd_xSi$ system.

Acknowledgements

The work done at Aoyama Gakuin University was supported by The Science Research Fund of the Japan Private School Promotion Foundation. A part of the work performed at Aoyama Gakuin University was supported by The Private School High-Tech Research Center Program of The Ministry of Education, Science, Sports and Culture, Japan.

References

[1] R.J. Cava, H. Takagi, B. Batlogg, H.W. Zandbergen, J.J. Krajewski, W.F. Peck Jr, R.B. van Dover, R.J. Felder, T. Siegrist, K. Mizuhashi, J.O. Lee, H. Eisaki, S.A. Carter, S. Uchida, Nature 367 (1994) 146.
[2] R.J. Cava, H. Takagi, H.W. Zandbergen, J.J. Krajewski, W.F. Peck Jr., T. Siegrist, B. Batlogg, R.B. van Dover, R.J. Felder, K. Mizuhashi, J.O. Lee, H. Eisaki, S. Uchida, Nature 367 (1994) 252.
[3] T. Siegrist, H.W. Zandbergen, R.J. Cava, J.J. Krajewski, W.F. Peck Jr., Nature 367 (1994) 254.
[4] E. Hovestreydt, N. Engel, K. Klepp, B. Chabot, E. Parthe, J. Less-Common Met. 86 (1982) 247.
[5] T. Fujita, T. Suzuki, S. Nishigori, T. Takabatake, H. Fujii, J. Sakurai, J. Magn. Magn. Mater. 108 (1992) 35.
[6] Y. Nagata, K. Sodeyama, S. Yashiro, H. Sasaki, H. Samata, T. Uchida, M.D. Lan, J. Alloys Comp. 281 (1998) 112.
[7] I. Shirotani, Y. Konno, Y. Okada, C. Sekine, S. Todo, T. Yagi, Solid State Commun. 108 (1998) 967.
[8] H. Wiesmann, M. Gurvitch, H. Lutz, A.K. Ghosh, B. Schwarz, M. Strongin, P.B. Allen, J.W. Halley, Phys. Rev. Lett. 38 (1977) 782.
[9] S. Ramakrishnan, K. Ghosh, A.D. Chinchure, V.R. Marathe, G. Chandra, Phys. Rev. B 52 (1995) 6784.
[10] E.S. Hellman, E.H. Hartford Jr., Phys. Rev. B 47 (1993) 11346.
[11] S. Ramakrishnan, K. Ghosh, A.D. Chinchure, V.R. Marathe, G. Chandra, Phys. Rev. B 52 (1995) 6785.
[12] R.M. White, in: Quantum Theory of Magnetism, MacGraw-Hill, New York, 1970, p. 86.
[13] A.H. Wilson, in: The Theory of Metals, Cambridge University Press, London, 1965, p. 168.